AIChE

Characterization of the Devolatilization Rate of Solid Fuels in Fluidized Beds by Time-Resolved Pressure Measurements

R. Solimene, R. Chirone and P. Salatino
Istituto di Ricerche sulla Combustione - CNR, Dipartimento di Ingegneria Chimica, Università degli Studi di Napoli Federico II Piazzale Tecchio 80, 80125 Napoli, Italy

DOI 10.1002/aic.12607
Published online April 27, 2011 in Wiley Online Library (wileyonlinelibrary.com).

The characterization of volatile matter (VM) release from solid fuel particles during fluidized-bed combustion/gasification is relevant to the assessment of the reactor performance, as devolatilization rate affects in-bed axial fuel segregation and VM distribution across the reactor. An experimental technique for the characterization of the devolatilization rate of solid fuels in fluidized beds is proposed. It is based on the analysis of the time series of pressure measured in a bench-scale fluidized-bed reactor as VM is released from a batch of fuel particles. A remarkable feature of the technique is the possibility to follow fast devolatilization with excellent time-resolution. A mathematical model of the experiment has been developed to determine the time-resolved devolatilization rate, the devolatilization time and the volume-based mean molecular weight of the emitted volatile compounds. Devolatilization kinetics has been characterized for different solid fuels over a broad range of particle sizes. © 2011 American Institute of Chemical Engineers *AIChE J,* 58: 632–645, 2012
Keywords: devolatilization, pyrolysis, reaction kinetics, fluidized bed, coal, biomass

Introduction

The growing interest for the fluidized bed combustion/gasification of nonfossil solid fuels (biomass, peat, municipal, agricultural and industrial wastes) and low-rank coal emphasizes the importance of a better understanding of the kinetics of fuel devolatilization in fluidized beds. Despite extensive literature that has been published on this subject,[1] the mechanisms controlling the release of volatile matter under fluidized-bed processing conditions and its relevance to the reactor performance have not been fully clarified and are still the subject of experimental and theoretical investigation.

Uneven axial and radial distribution of volatile matter in the fluidized-bed combustor is commonly experienced in industrial units and is reflected by uneven profiles of heat release and enhanced pollutant formation/emission. In-bed emission of volatile matter is responsible for the formation of ''endogenous'' volatile bubbles[2–3] as a consequence of the hydrodynamic interaction between gas-emitting particles and the fluidized suspension. Endogenous bubbles enhance axial segregation of fuel particles at the bed surface and favor the establishment of ''stratified'' combustion.[2–10] On the other hand, the competition between fuel devolatilization and radial solids mixing crucially affects the radial distribution of volatile matter across the reactor and emphasizes the relevance of the devolatilization kinetics to volatile matter segregation. Short devolatilization times promote the release of volatile matter above the bed and close to the fuel feeding points,[11–13] when mixing with the fluidizing gas eventually takes place along the freeboard (in bubbling fluidized-bed reactors), or the riser (in circulating fluidized-bed reactors).

The complex phenomena associated with thermal degradation of a solid fuel, involving pyrolytic reactions, intraparticle heat and mass transfer and particle fragmentation, have

Correspondence concerning this article should be addressed to R. Solimene at solimene@irc.cnr.it.

been largely scrutinized.[14–36] Devolatilization of fine particles is typically controlled by the intrinsic kinetics of pyrolytic reactions, often represented by multiple-parallel-reaction models with a continuous distribution of activation energies (DAEM).[37–39] An alternative approach to model the kinetics of pyrolytic reactions is based on the use of a single n^{th} order reaction rate equation with Arrhenius-type temperature dependence.[40] Unsteady heat conduction into the particle, in a thermally thick regime, or diffusion of volatile species toward the external surface may become the dominant mechanism for coarse particles. The transition between the two regimes depends on the effectiveness of heat transfer in the particle boundary layer and inside the particle itself. Under this respect it is worth recalling that external heat transfer is very efficient in fluidized-bed reactors, yielding particle heating rates as high as 10^4 K/s under typical combustion/gasification conditions.

Different experimental techniques have been used to measure the devolatilization rate of fuel particles. Thermogravimetric analysis, in both vertical and horizontal tube furnaces,[41–43] or drop-tube furnaces are valuable tools for the study of devolatilization at, respectively, moderate temperature/small heating rate and high-temperature/large heating rate. However, these types of experiments do not reflect conditions typical of fluidized-bed processing of fuel particles.[42] Experiments based on "*in situ*" diagnostics of devolatilization in fluidized beds better reproduce the key features of devolatilization during practical fluidized-bed combustion or gasification. Two such techniques—the flame period and flame extinction time methods—are based on the detection of volatile flames around the devolatilizing fuel particles by either visual observation[7,35,42,44–47] or detection of UV emission.[48] The flame period is the time interval during which volatile flames are visible above the bed surface, whereas the flame extinction time is defined as the time elapsed from injection of the particle into the bed until the volatile flame ultimately vanishes. Both techniques, based on the detection of the presence of flames, involve a certain level of inaccuracy mostly associated with the precise detection of the beginning and of the end of devolatilization. On the other hand, devolatilization of coarse fuel particles, of size larger than a few millimeters, can also be directly characterized by periodic sampling of fuel particles from the fluidized bed at regular time intervals, followed by the analytical determination of the residual volatile matter in the samples.[16,32,49] Techniques based on the analysis of the time-resolved concentration of gases released during devolatilization[30,42,50–57] are almost as simple as the flame methods. When pyrolysis occurs in inert conditions, devolatilization times corresponding to either 50 or 95% conversion degrees are usually calculated by the analysis of the time-resolved methane concentration measured at the exhaust.[50–51] When pyrolysis is carried out under oxidizing conditions, the devolatilization rate and time may be assessed by consideration of the time series of carbon dioxide and oxygen concentrations at the exhaust.[30,42,52–56] The time/temperature history of the fuel particle can be further analyzed since its injection in the fluidized bed to assess the progress of drying, devolatilization and char burn-out.[26–27,46,58–60] Ross et al.[59] proposed to take the time interval between fuel particle injection and the time at which the center of the particle reaches the bed temperature as a measure of the devolatilization time. The possibility to correlate the progress of devolatilization with the pressure increase measured in a fluidized-bed reactor was also investigated with reference to a biomass fuel.[28,54,61]

Devolatilization is closely correlated with the size of the fuel particle. The correlation is usually expressed according to a power-law dependence whose exponent reflects the devolatilization-controlling mechanism. The large variability of fuel particle sizes in the feedings of fluidized-bed combustors and gasifiers emphasizes the need for a reliable characterization of the devolatilization rate and mechanisms over a broad range of particle sizes, in particular in the <1 mm size range for which data are definitely lacking.

In this study, a novel diagnostic technique for "*in situ*" characterization of coal devolatilization in gas-fluidized beds is proposed. It is based on the analysis of the pressure time-series measured in a bench-scale fluidized bed equipped with a calibrated flow restriction at the exhaust. The concept underlying the experimental method is that devolatilization rate can be correlated with the pressure level in the reactor as it is modified by the incremental flow of volatile matter issuing from the reactor during devolatilization of a batch of fuel particles. Compared with alternative methods, this experimental technique is characterized by an inherently fine time-resolution. This feature enables accurate characterization of the devolatilization kinetics even when devolatilization is extremely fast, as is the case for fuel particles in the 0.1–1 mm size range.

Experimental

Experimental apparatus

The experimental apparatus (Figure 1) consists of a stainless steel fluidized-bed reactor 0.5 m high, 0.017 m ID. The top flange of the reactor bears two holes. One hole is used to host a movable pressure tap in the column. A high-precision (accuracy better than 0.06 mbar) piezo-resistive electronic pressure transducer with small-time response (smaller than 1 ms), and 70 mbar full-scale was connected to the pressure probe to measure the time-resolved gas pressure in the reactor. The pressure signal was acquired by means of a data acquisition unit consisting of an A/D converter (National Instruments PCI 6034E) and a personal computer. The other hole is used to host a probe 0.49 m long bearing a thermocouple (K-type) to measure the temperature in the fluidized bed about 0.01 m above the distributor plate. An exhaust duct and a fuel particle feeding duct are also welded to the column. The former (0.006 m OD) is perpendicular to the column axis at a level of 0.026 m from the top flange and is connected to a vent. The latter (0.0095 m ID, 0.014 m OD and 0.13 m long) is welded to the column with an inclination of about 45° with respect to the column axis, 0.08 m below the top flange. The feeding duct is equipped with a double-valve system in order to inject batches of fuel particles over bed with minimal perturbation of the reactor overpressure.

The fluidizing gas was metered through a wind box filled with a packing and a high-pressure-drop porous gas distributor made of sintered steel. The wind box packing makes preheating of the fluidizing gas more effective and, together

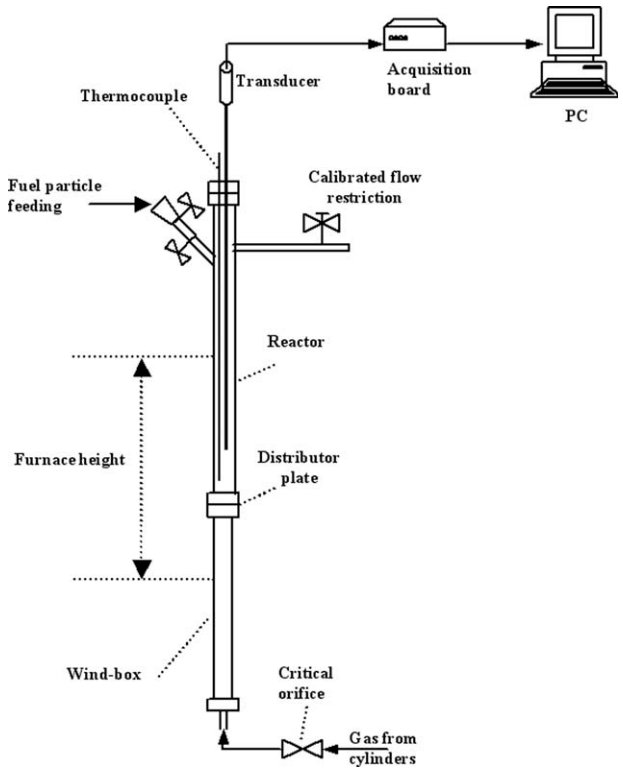

Figure 1. The experimental apparatus.

with the distributor plate, makes the gas flow to be evenly distributed across the bed.

Fluidizing gas was technical nitrogen from cylinders. The fluidizing gas-flow rate was established by setting the upstream pressure of a critical orifice located along the gas feeding line. The orifice (0.187 mm dia.) was typically operated in critical flow conditions. The upstream relative pressure varied between 1 and 3.5 bar.

The reactor was operated at a pressure slightly larger than atmospheric pressure by means of a calibrated flow restriction at the exhaust consisting of an orifice with an adjustable cross section. This restriction was periodically cleaned to remove tar deposits generated during fuel pyrolysis.

The reactor could be steadily operated at temperatures up to 900°C by means of a cylindrical oven (Heraeus 1 kW) 0.4 m high equipped with a PID temperature control system. The parts of the column lying outside the oven were insulated to prevent heat loss.

Materials

Bed material was silica sand in the 355–400 μm size range. The bed inventory was 13 g corresponding to a static bed height of about 0.04 m and, correspondingly, to an aspect ratio of about 2.35. These operating conditions were selected so as to limit the occurrence of slugging.[62] The incipient fluidization velocity measured at 1,123 K was about 0.065 m/s, in good agreement with Wen and Yu.[63]

Samples consisted of different fossil and nonfossil solid fuels whose properties are reported in Table 1. Two coals were tested: a South-African coal characterized by finely dispersed ash in the carbon matrix, and a Polish coal which instead presents frequent occurrence of coherent ash skeletons. Granulated sewage sludge and wood chips were also investigated. The initial particle size was varied between 0.1 and 6 mm, compatible with the cross sections of the column and of the feeding duct. Based on previous experience, the occurrence of primary fragmentation was unlikely for all the fuels in the particle-size range investigated[20,22,56,64–65] with the exception of wood chips which displayed moderate fragmentation of particles coarser than about 5 mm size.[66]

Experimental procedure

Pressure was continuously monitored in the fluidized-bed reactor during the experiments. Gas pressure inside the reactor increases during devolatilization as the incremental flow rate due to volatile matter emission flows across the calibrated flow restriction. The selection of the steady-state overpressure in the reactor, dictated by the flow rate of fluidizing gas and by the calibrated flow restriction at the exhaust, determines the time evolution of the phenomena. Very high overpressures emphasize the inherent dynamics of the vessel associated with the flow rate increase. On the other hand, small overpressures make detection of volatile matter emission less precise and reliable. After careful optimization, the best trade-off was found as an overpressure of about 9−10 mbar was established.

The temperature in the fluidized bed was kept constant at about 1,123 K. The fluidizing gas was nitrogen to rule out the influence of volatile matter and char combustion on the recorded pressure profiles. The upstream pressure at the critical orifice was kept at a constant value of about 2.5 bars. Correspondingly, the fluidizing gas velocity was 2.5 times the incipient fluidization velocity. At this velocity, the occurrence of slugging was prevented[62] and the background noise of pressure signals associated with fluctuations induced by bubbling was very limited.

The mass of each batch of fuel particles (with the exception of wood chips) was varied between 10 and 80 mg depending on the volatile matter content of the tested fuel, so that the amount of volatile matter was nearly constant (ca. 25 mg) in each experiment, regardless of the fuel type. The amount of volatile matter cumulatively emitted over the test was a trade-off between the establishment of an appreciable overpressure as a consequence of volatile matter emission and the need to prevent plugging of the calibrated flow

Table 1. Properties of the Tested Fuels

Fuel	South African coal	Polish coal	Granulated Sewage sludge	Wood chips
Proximate Analysis, $\%_w$ (as received)				
Moisture	7.4	3.0	10.8	14.4
Volatile Matter	21.8	27.7	51.8	68.4
Ash	12.9	5.9	32.7	0.4
Fixed Carbon	57.9	63.4	4.6	16.7
Ultimate Analysis, $\%_w$ (dry basis)				
Carbon	66.5	77.8	30.6	50.2
Hydrogen	4.4	4.5	4.6	6.2
Nitrogen	1.2	1.2	4.2	0.2
Sulphur	0.6	0.5	1.1	0.1
Ash	13.9	6.1	36.6	0.4
Oxygen (by difference)	13.3	9.9	22.9	42.9

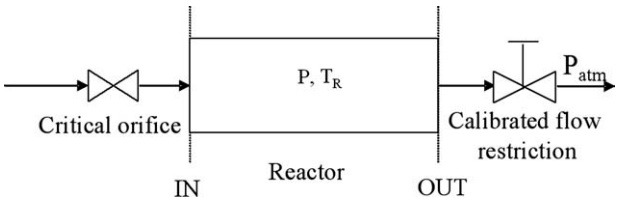

Figure 2. Schematic representation of the reactor.

restriction by tar deposits. Wood chips were fed as single particles of mass comprised between 2.5 and 25 mg.

The tests consisted of the injection of a batch of fuel particles in the fluidized bed followed by complete devolatilization. For each test the initial mass and size of the fuel particles were recorded. The pressure signal was continuously logged during the experiments at a sampling rate of 1,000 Hz by means of a purposely developed LabView program. Pressure time-series were eventually analyzed in the light of a model of the experiment (see following section) in order to determine the volatile emission rate as a function of time. The time for 95% devolatilization degree and the mean molecular weight of the emitted volatile compounds were computed from the raw data. For two fuels (South African coal and wood chips), the influence of the moisture content was also investigated by carrying out additional tests using batches of pre-dried samples.

Setup of the Data Post-Processing Procedure

The raw data consisting of the pressure time series were worked out to yield the devolatilization rates according to a model of the experiment, based on the flow diagram of Figure 2. Model equations consist of the transient mass balance on the reactor referred to two species: the fluidizing gas and the volatile matter.

Model assumptions

The following assumptions were made:

1. The mass flow rate of gas fed to the reactor is independent of the pressure inside the reactor. This assumption is justified by the consideration that the fluidizing gas supply line is equipped with an orifice operated at critical conditions. Accordingly, the mass-flow rate is dependent on the regulated upstream pressure only, regardless of the pressure establishing in the reactor;

2. The differential pressure between the reactor and the atmosphere is dominated by the calibrated flow restriction at the exhaust of the reactor, other sources of pressure drop being negligible;

3. Volatile matter behaves as a single compound having an average molecular mass that is taken constant along with devolatilization;

4. The gas phase is well-mixed inside the reactor;

5. The temperature of the fluidized bed is constant during devolatilization and not influenced by fuel particle injection and volatile matter emission;

6. The volumetric flow rate of gases at the exhaust is proportional to the difference between the reactor (P) and the atmospheric (P_{atm}) pressures

$$Q_{OUT} = K_p(P - P_{atm}) \tag{1}$$

where K_p is a proportionality constant;

7 The perfect gas-law holds for both the fluidizing gas and the volatile compounds

$$P = \frac{\rho_{gas} R_g T_R}{M_{gas}} + \frac{\rho_{vol} R_g T_R}{M_{vol}} \tag{2}$$

where ρ_{gas}, ρ_{vol}, T_R, R_g, M_{gas} and M_{vol}, are, respectively, the density of fluidizing gas and volatile matter, the reactor temperature, the gas-law constant and the molecular weights of fluidizing gas and volatile matter. The validity of this assumption with specific reference to the volatile compounds will be further reconsidered in the Discussion section in the light of the experimental results.

Model equations

The transient mass balance on the two species reads

$$\begin{cases} V_R \frac{d\rho_{gas}}{dt} = \dot{m}_0 - \rho_{gas}(t) Q_{OUT}(t) \\ V_R \frac{d\rho_{vol}}{dt} = \dot{m}_v(t) - \rho_{vol}(t) Q_{OUT}(t) \end{cases} \tag{3}$$

$$\text{I.C.} : \begin{cases} \rho_{gas}(t = 0) = \rho_{IN} = \rho_{gass} \\ \rho_{vol}(t = 0) = 0 = \rho_{vols} \end{cases} \tag{4}$$

where V_R is the reactor volume, $\dot{m}_0$ is the mass-flow rate of the fluidizing gas, and $\dot{m}_v(t)$ is the mass-flow rate of emitted volatiles.

The system of nonlinear equations (Eq. 3) can be rearranged by taking into account Eq. 2 to yield a single nonlinear ordinary differential equation in terms of the reactor pressure

$$\begin{cases} V_R \frac{dP}{dt} + K_p P(P - P_{atm}) = R_g T_R \left(\frac{\dot{m}_0}{M_{gas}} + \frac{\dot{m}_v(t)}{M_{vol}} \right) \\ P(t = 0) = P_0 \end{cases} \tag{5}$$

where P_0 is the pressure established in the reactor at steady state, i.e., before feeding the fuel batch. This is also the final value of the reactor pressure once devolatilization is complete. Equation 5 can be simplified once the nonlinear term $P(P - P_{atm})$ is linearized around the initial condition (P_0)

$$P(P - P_{atm}) \cong P(2P_0 - P_{atm}) - P_0^2 \tag{6}$$

Accordingly, Eq. 5 can be rearranged into the linearized model

Table 2. Model Input Variables

Geometrical features of the reactor and operating conditions	
Reactor volume, V_R, m^3	$1.135 \cdot 10^{-4}$
Reactor temperature, T_R, K	1123
Initial reactor pressure, P_0, mbar	1023
Proportionality constant of Equation (1), K_p, $m^3/(s\ mbar)$	$3.691 \cdot 10^{-6}$
Devolatilization process	
Volatile matter mass, m_v, mg	18
Characteristic time constant, τ, s	0.1, 0.5, 1

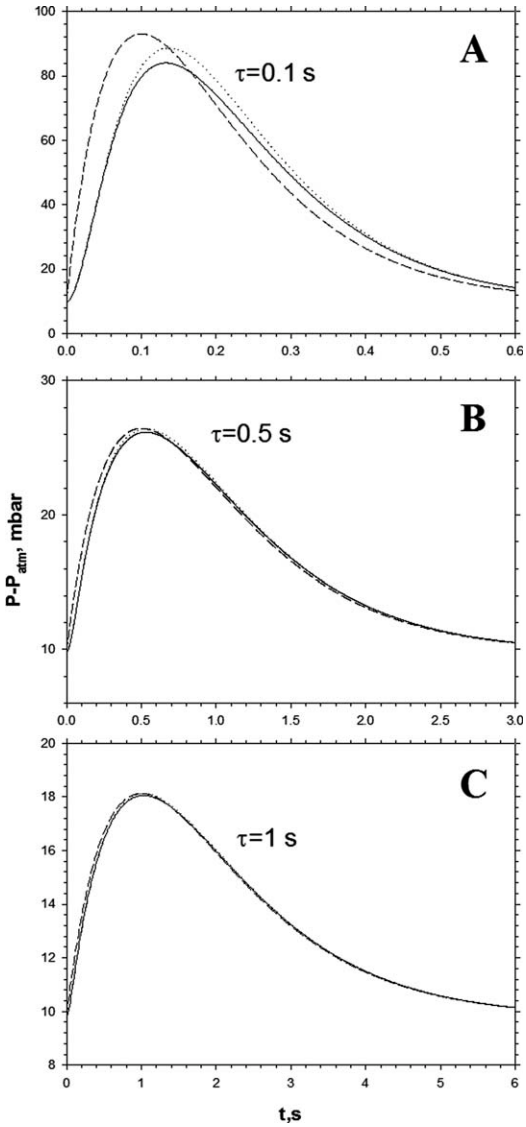

Figure 3. Model results: time-resolved relative pressure for different values of the devolatilization time constant.

Solid line: nonlinear model (Eq. 5); dotted line: linearized model (Eq. 7); dashed line: quasi-steady state approximation (Eq. 9). A: $\tau = 0.1$ s; B: $\tau = 0.5$ s; C: $\tau = 1$ s.

$$\begin{cases} \tau_f \frac{dP}{dt} + P = P_0 + \frac{R_g T_R \dot{m}_v(t)}{M_{vol} K_p (2P_0 - P_{atm})} \\ P(t=0) = P_0 \end{cases} \quad (7)$$

where the time constant τ_f is

$$\tau_f = \frac{V_R}{K_p(2P_0 - P_{atm})} \quad (8)$$

It is worth noting that, with a proper choice of the baseline reactor pressure P_0, the time constant τ_f can be made much smaller than the reactor space-time $\frac{V_R}{Q_{OUTO}} \simeq \frac{V_R}{K_p(P_0 - P_{atm})}$, a feature that is important in view of the possibility to follow rapid devolatilization.

If the time constant τ_f is small with respect to the time scale of particle devolatilization, the quasi-steady state approximation leads to a simplified version of Eq. 7 according to which the molar flow rate of emitted volatiles can be linearly correlated with the instantaneous value of the reactor overpressure

$$\frac{\dot{m}_v(t)}{M_{vol}} = \frac{K_p(2P_0 - P_{atm})}{R_g T_R}(P(t) - P_0) \quad (9)$$

The mean molecular weight (M_{vol}) of the volatile compounds can be calculated as

$$M_{vol} = \frac{m_{v0}}{\int_{t_i}^{t_f} \frac{\dot{m}_v(t)}{M_{vol}} dt} = \frac{m_{v0}}{\int_{t_i}^{t_f} \frac{K_p(2P_0 - P_{atm})}{R_g T_R}(P(t) - P_0) dt} \quad (10)$$

where m_{v0} is the mass of volatile matter in the fuel sample, and t_i and t_f are the times at which fuel injection and leveling off of reactor pressure take place, respectively. The value of t_f was taken as the time at which departure of P with respect to P_0 was less than 1%.

A characteristic devolatilization time t_{D95} corresponding to 95% volatile matter emission is calculated from the condition

$$0.95 \int_{t_i}^{t_f} \frac{\dot{m}_v(t)}{M_{vol}} dt = \int_{t_i}^{t_{D95}} \frac{\dot{m}_v(t)}{M_{vol}} dt \Leftrightarrow$$
$$0.95 \int_{t_i}^{t_f} \frac{K_p(2P_0 - P_{atm})}{R_g T_R}(P(t) - P_0) dt$$
$$= \int_{t_i}^{t_{D95}} \frac{K_p(2P_0 - P_{atm})}{R_g T_R}(P(t) - P_0) dt \quad (11)$$

Assessment of the postprocessing procedure

The mathematical model of the experiment has been used to verify:

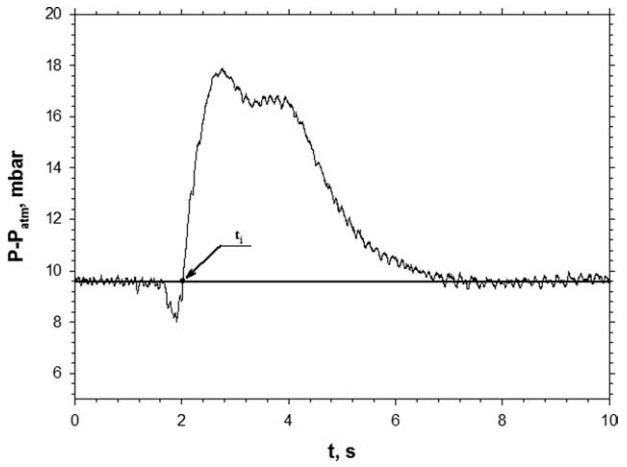

Figure 4. Typical time-resolved relative pressure profile measured in the reactor during the devolatilization of a batch of South-African coal particles (total mass of the batch: 82.4 mg; particle-size range: 1.18–1.40 mm).

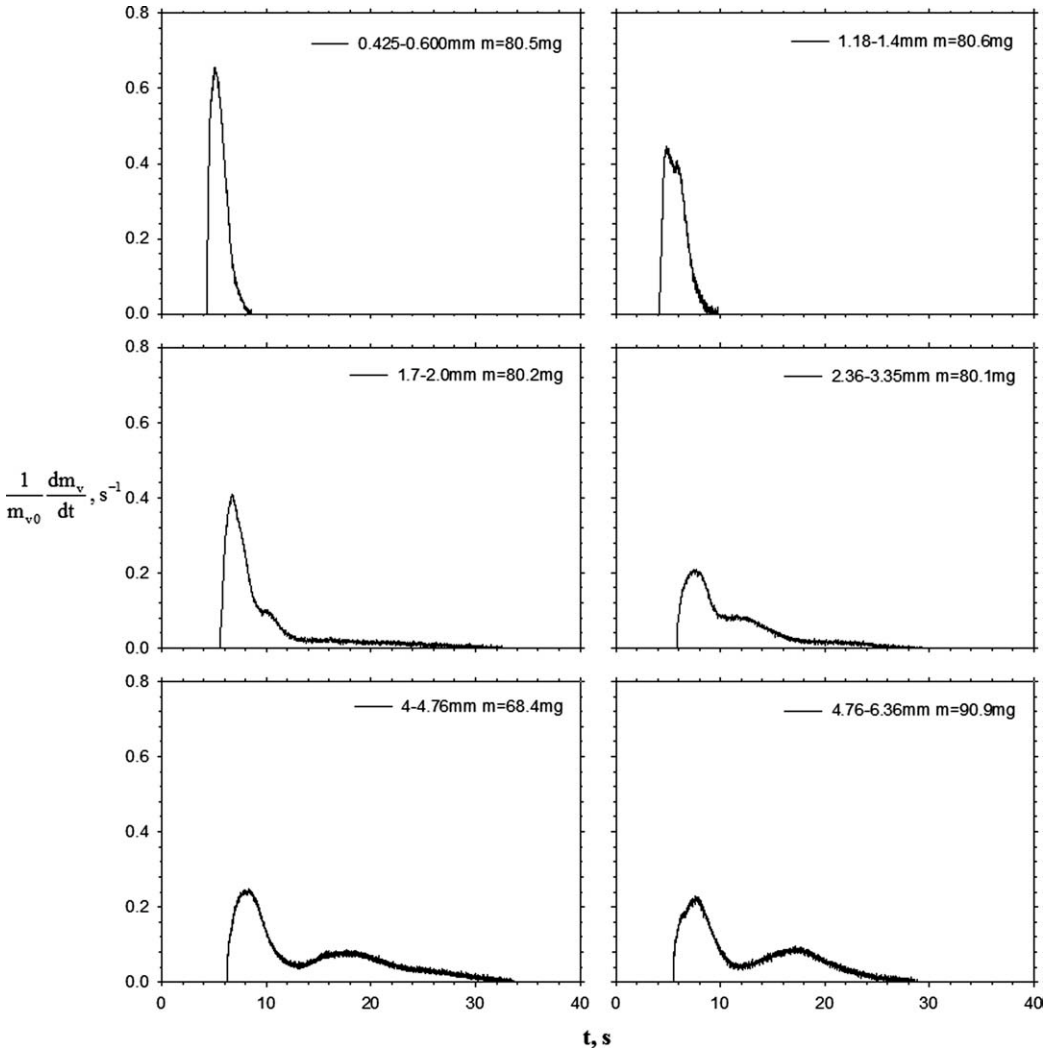

Figure 5. Devolatilization rate as a function of time for batches of South-African coal: influence of initial particle size.

- the possibility to compute the devolatilization rate from deconvolution of time-resolved pressure profiles, getting rid from the inherent dynamics of the reactor, especially when devolatilization is fast;
- the limits within which the pseudo-steady state version of the model (Eq. 9) can be used in place of the more general solution of the differential Eq. 5.

To this end, the reactor geometrical parameters and operating conditions described in the Experimental section were adopted. The selected value of the baseline reactor overpressure ($P_0 - P_{atm} = 9 - 10$ mbar) introduces an error related to linearization of the differential Eq. 5, which is less than 1 mbar for overpressures in the reactor of about 40 mbar. On the other hand, the time constant τ_f appearing in Eq. 7 is of the order of 0.03 s. These figures indicate that for small deviations of the reactor overpressure with respect to the baseline and for devolatilization processes longer than 1 s, the inherent dynamics of devolatilization can be effectively deconvoluted from the dynamic response of the reactor and data post processing can be based on the linearized Eq. 9.

The data postprocessing procedure has been tested by applying it to a simulated devolatilization process. To this end the devolatilization rate has been simulated according to the simple expression

$$\dot{m}_V(t) = \frac{m_{v0}t}{\tau^2}\exp\left(-\frac{t}{\tau}\right) \tag{12}$$

where τ has the meaning of a characteristic devolatilization time scale, which provides a reasonable simulated devolatilization profile.[64] The nonlinear differential Eq. 5 has been solved to obtain $P(t)$, with $\dot{m}_v$ (t) given by Eq. 12. A fourth-order Runge-Kutta algorithm with adaptive integration step size was implemented in the MathCad® environment. The model input variables adopted are shown in Table 2. Figure 3 reports the pressure time series computed according to Eq. 5 for different values of the characteristic devolatilization time τ. The same figure reports the pressure time series computed according to the linearized model (Eq. 7) and the profiles computed according to the quasi-steady state approximation (Eq. 9). The comparison suggests that: (1) the nonlinear and

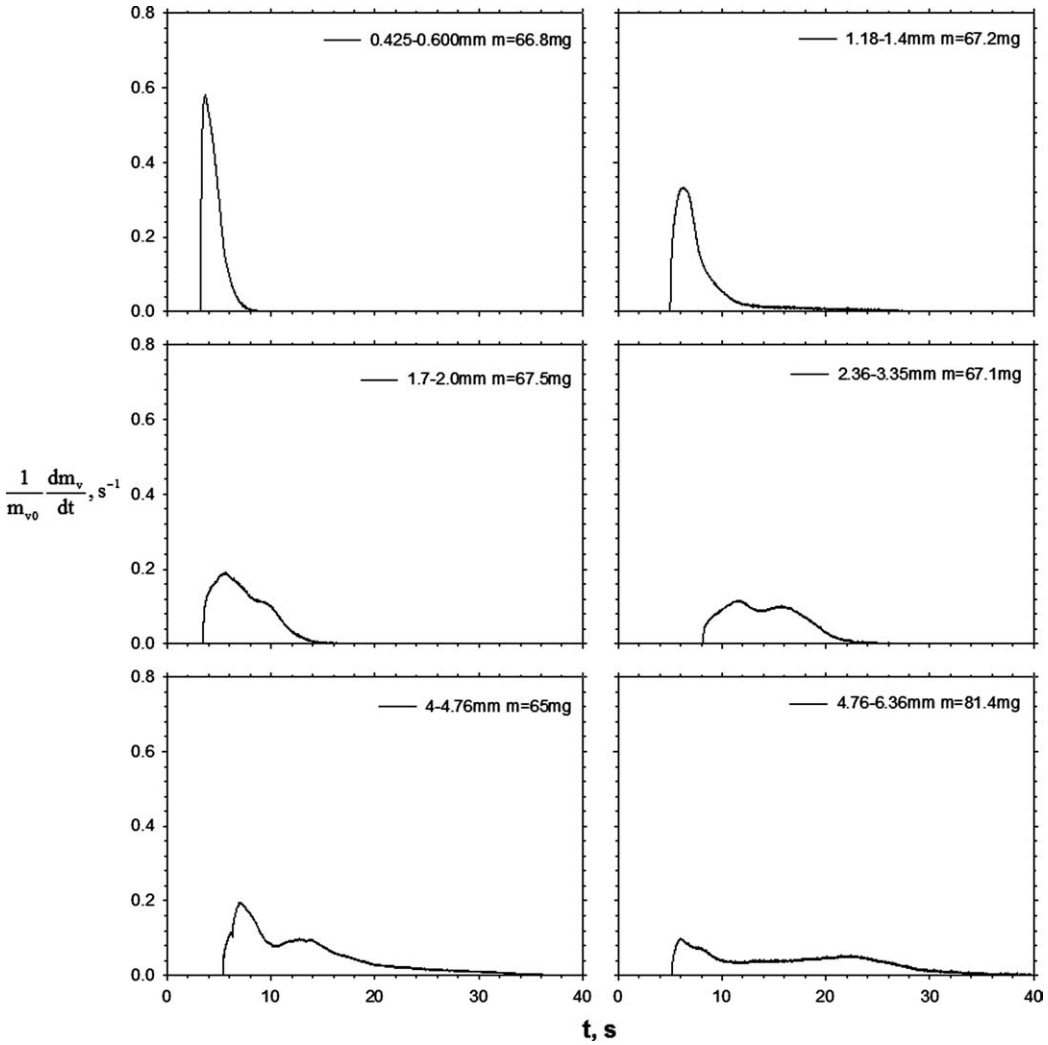

Figure 6. Devolatilization rate as a function of time for batches of Polish coal: influence of initial particle size.

linearized models yield similar predictions, except for some departures of the maximum overpressure for time scales τ of 0.1 s and smaller; and (2) the quasi-steady state approximation (Eq. 9) is only justified for devolatilization time scales much larger than τ_f (say, $\tau \geq 10\ \tau_f$).

Results of these computations have been taken into account to optimize the postprocessing procedure of the experimental data reported in the following. In particular:

- for devolatilization time scales of 0.5 s and longer, the quasi-steady state approximation applied to the linearized model is adopted (Eq. 9);
- for devolatilization time scales smaller than 0.5 s, deconvolution of pressure time series to get rid of the inherent dynamics of the fluidized-bed reactor is necessary.

Experimental Results

Bituminous coals

Figure 4 reports the typical pattern of the time-resolved reactor overpressure recorded during the devolatilization of a batch of a South African bituminous coal. The mass of the batch is of about 80 mg of coal particles sieved in the 1.4–1.7 mm size range. The reactor overpressure, initially equal to the preset baseline value (ca. 10 mbar), abruptly decreases as the fuel sample is fed to the reactor to increase, thereafter, up to a maximum of about 18 mbar in about 0.8 s. A pronounced shoulder is displayed just after the maximum (ca. 16 mbar), then the reactor overpressure decays to the baseline value over about 5 s. The pressure decrease that immediately follows sample feeding is related to the perturbation of the steady overpressure due to particle injection and to some cooling of the bed in contact with the fuel particles at ambient temperature. For the case considered in Figure 4, the dynamics of devolatilization is slow enough to make the quasi-steady state approximation applicable (devolatization time scale longer than 0.5 s). Accordingly, Eq. 9 could be used to work out the pressure time series.

Figure 5 compares the devolatilization rates, expressed as $\frac{1}{m_{v0}}\frac{dm_v}{dt}$, worked out from data recorded in tests with batches of South African coal particles of different sizes according to the postprocessing procedure described previously. The mass of each batch was kept constant at about 80 mg. As the size of the fuel particles is changed, the following features can be recognized:

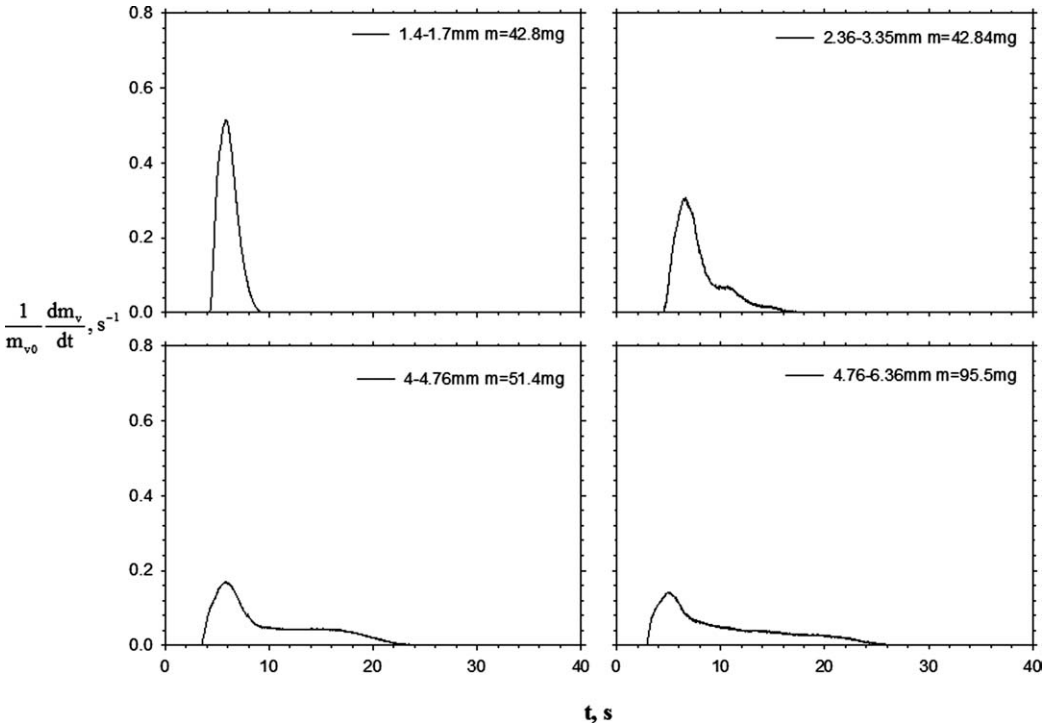

Figure 7. Devolatilization rate as a function of time for batches of granulated sewage sludge: influence of initial particle size.

1. The sudden pressure drop associated with particle feeding becomes more pronounced as the particle size is decreased, as a consequence of faster heat transfer between the ''cold'' fuel particles and the hot bed;

2. The rise of the devolatilization rate becomes steeper as the particle size decreases. Again this is interpreted as a consequence of the faster heating of smaller particles characterized by smaller Biot number;

3 The decay of the devolatilization rate toward the baseline is faster, the smaller the fuel particles;

4 The shoulder observed in Figure 4 is delayed as the particle size increases, eventually yielding a second maximum for fuel particles coarser than 2.3 mm. On the contrary,

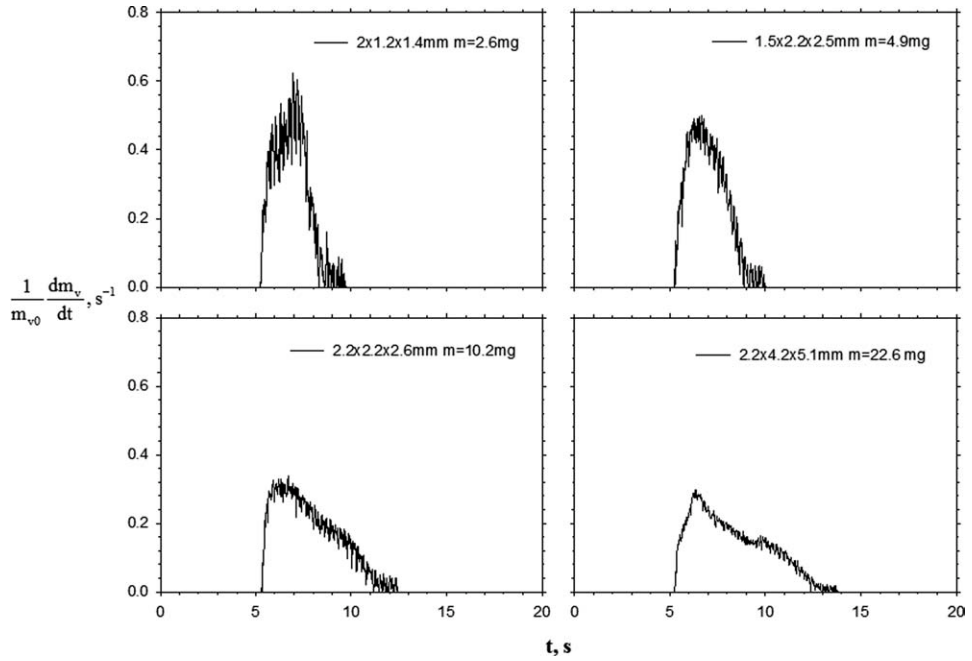

Figure 8. Devolatilization rate as a function of time for batches of wood chips: influence of initial particle size.

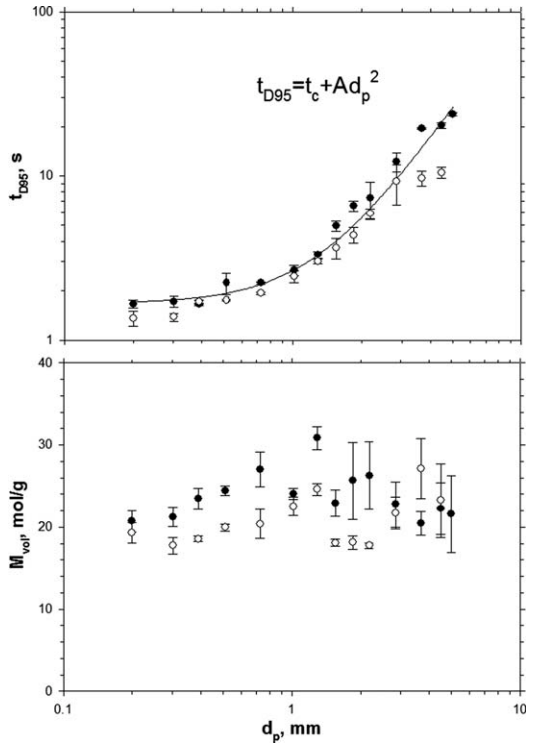

Figure 9. Devolatilization time and mean molecular weight as a function of the initial fuel particle size.

Fuel: South African coal; close circles: raw fuel; open circles: pre-dried fuel.

the shoulder merges with the devolatilization rate peak and vanishes as the particle size is decreased below about 1 mm.

The time-resolved devolatilization rates measured during experiments carried out with batches of Polish bituminous coal particles are reported in Figure 6. The mass of each batch was about 70 mg in this case. The general features of the devolatilization rates recorded with the Polish coal closely reproduce those observed with the South African coal. For $d_p < 0.5$ mm, the duration of devolatilization is nearly the same, the maximum overpressure being slightly larger for the Polish coal. In the coarse of particle-size range (1 mm $< d_p <$ 5.5 mm), devolatilization takes a slightly longer time to be completed as compared with the South African coal sample. Distinct maxima are observed also in this case. For the coarsest particle sizes ($d_p > 2$ mm), Polish coal is characterized by a more uniform and steady emission of volatile matter with respect to the South African coal. This feature can be related to the finding that Polish coal, unlike South African coal, is characterized by frequent occurrence of coherent ash skeletons, possibly affecting transient heat transfer within the particle.

It can be speculated that the existence of distinct maxima in the devolatilization profiles of coarse particles of the two coals tested, merging into a shoulder as one moves toward finer particles, may be related to the existence of multiple sequential stages of gas emission. Such occurrence has been already reported in the literature and related to the coexistence in the coal structure of "loose" and "tight" fragments released at different stages along devolatilization.[39,67,68]

Granulated sewage sludge

Figure 7 reports the time-resolved devolatilization rate measured during devolatilization of batches of granulated sewage sludge. Batches of about 45 mg of particles belonging to different size ranges were tested. Instantaneous feeding of sludge particles smaller than about 1 mm could not be accomplished, due to their filamentous nature which promoted particle agglomeration and plugging of the feeding duct. So, only particles coarser than 1 mm were tested.

The devolatilization patterns of granulated sewage sludge have some distinctive features when compared with the phenomenology reported for the bituminous coals. The abrupt pressure drop associated with fuel injection is less pronounced in this case, and the eventual pressure rise slower. It might be speculated that the large ash content and the coherent nature of the ash skeleton which establish within the particle already during devolatilization negatively affect intraparticle heat transfer. A remarkable feature of the devolatilization profiles is represented by the shoulder (at $d_p = 2$ mm) which extends to become a prolonged plateau (ca. 2 s for a 3 mm particle, 15 s for a 5 mm particle) in the late stage of particle devolatilization. Again, this peculiar devolatilization pattern could be explained by considering the presence of a coherent ash skeleton across which affect conductive heat transfer and flow of volatile matter in coarse particles.

Wood chips

Figure 8 shows the time-resolved devolatilization rates measured in the reactor during the pyrolysis of single wood

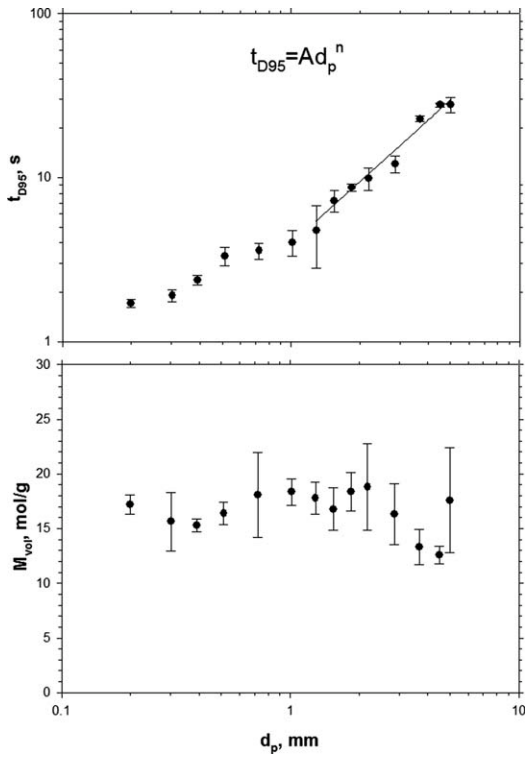

Figure 10. Devolatilization time and mean molecular weight as a function of the initial fuel particle size.

Fuel: Polish coal.

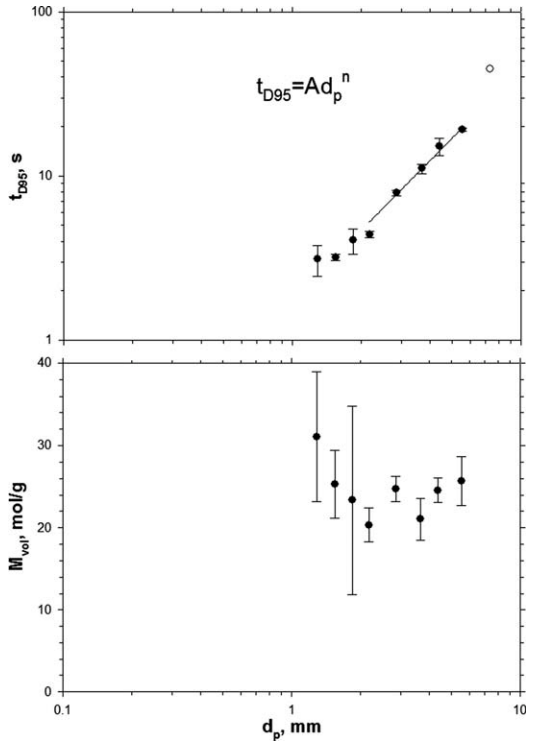

Figure 11. Devolatilization time and mean molecular weight as a function of the initial fuel particle size.

Fuel: granulated sewage sludge. The open circle is a data point obtained with the same material and the diagnostic technique based on CO_2.[56]

chips of different size and mass (between about 2.5 and 25 mg). The initial pressure rise is steeper, when compared with the other tested fuels, and the overall duration of the devolatilization process is shorter. A very small shoulder can be detected in profiles referred to the coarsest sample, possibly related to multiple sequential pyrolysis stages. Unlike the bituminous coals, no multiple peaks show up in this case.

Discussion

Devolatilization time vs. particle size

The time-resolved devolatilization rates have been worked out according to the postprocessing procedure (Eqs. 10 and 11) to estimate: (1) the time interval (t_{D95}) corresponding to 95% volatile matter release; and (2) the mean molecular weight (M_{vol}) of the emitted volatiles. The values are reported in Figures 9–12 as a function of the initial mean size of the fuel particles. For two fuels (South African coal and wood chips) data obtained with both raw and pre-dried fuel batches are reported.

As expected, the devolatilization time increases as the particle size increases for all the fuels tested, though differences can be recognized in the various cases. Pre-drying of fuel batches moderately affects the devolatilization time, which becomes shorter by 10–20% after predrying over the entire range of particle sizes.

Data points referring to the South African bituminous coal samples display a double-asymptotic pattern of the plot of t_{D95} vs. dp (Figure 9):

1. For fine particles the devolatilization rate is controlled by intrinsic kinetics of pyrolytic reactions and the devolatilization time does not depend on particle size;

2. For coarse particles the devolatilization rate is controlled by intraparticle heat transfer in the "thermally thick" regime. The devolatilization time scales with particle size to a power of $n = 2$.

Accordingly, data points for this coal were well correlated by the equation

$$t_{D95} = t_c + A\, d_p^2 \tag{13}$$

where t_c is a characteristic time related to the intrinsic devolatilization kinetics, and A is a proportionality constant embodying the effects of transient heat (and mass) transfer within the particle, as well as devolatilization kinetics. Regression analysis over all the data points yielded the best fit values of t_c and A reported in Table 3.

The double-asymptotic pattern of Figure 9 cannot be recognized in plots relative to the Polish bituminous coal, the granulated sludge and the wood chips. In particular, the limiting asymptote corresponding to small particle sizes ($t_{D95} \rightarrow t_c$) is not observed or is only partly approached within the range of particle size tested. It can be speculated that this limiting regime would be established with particles even

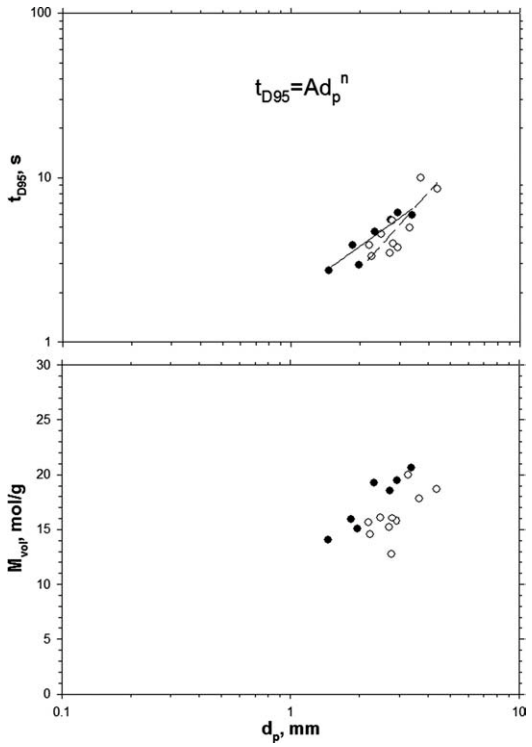

Figure 12. Devolatilization time and mean molecular weight as a function of the initial fuel particle size.

Fuel: wood chips; close circles/solid line: raw fuel; open circles/dashed line: pre-dried fuel.

Table 3. Fitting Constants of Equations (13 and 14)

Fuel	t_c, s	A, s/mm^n	n, -
South-African coal	1.67	0.98	2
Polish coal	-	3.98	1.25
Sewage sludge	-	1.77	1.41
Wet wood chips	-	1.92	1
Dry wood chips	-	0.94	1.56

finer than the minimum size tested in this campaign. For these fuels data points have been correlated by the equation

$$t_{D95} = Ad_p^n \tag{14}$$

yielding the best fit values of A and n reported in Table 3.

Figure 13 collectively reports t_{D95} vs. dp data points for all the fuels tested. Data points obtained in a previous study[56] with a different technique (analysis of CO_2 emissions at the exhaust) for pelletized biogenous fuels in the 7–10 mm size range are also shown. Moreover, the Figure reports plots of selected published correlations for the devolatilization time of coal and biomass particles.[42,59–60] Comparison of the data points suggests that the average devolatilization rate decreases in the order: wood chips > granulated sewage sludge > South African coal > Polish coal. Devolatilization times t_{D95} as short as 1.5 s could be measured with excellent confidence and reproducibility. This was possible due to a remarkable feature of the proposed technique: the inherently good time resolution of the method based on the dynamical analysis of the pressure time series. For the very same reason, the analysis of the devolatilization kinetics in a fluidized bed could effectively be accomplished with particles sizes as small as 0.2 mm. This is well below the minimum particle size, typically 1–3 mm, for which the devolatilization rate can be confidently measured using alternative methods. It has been reported that techniques based on the analysis of the time-resolved concentration profile of gaseous species released during devolatilization present significant measurement errors due to gas transport and diffusion in the sampling lines for fuel particle sizes smaller than 3 mm.[42] The span of the literature correlations reported in Figure 13 (2 mm $< d_p <$ 15 mm) reflects the typical particle-size range within which alternative methods for the characterization of the devolatilization rate have been employed.

Data in Figure 13 are helpful to assess the relevance of segregation of volatile matter in industrial-scale fluidized bed combustors/gasifiers. Axial segregation of gas-emitting fuel particles and "stratified" combustion are promoted by devolatilization and formation of "endogenous" bubbles of volatile matter.[2–10] Poor lateral dispersion of volatile matter from the fuel feeding ports arises from the combination of short devolatilization times and long time scales of fuel particle lateral spreading.[11] The effectiveness of lateral dispersion of volatile matter across the combustor is assessed by comparing the characteristic time of solids-lateral mixing (t_{mix}) with the characteristic devolatilization time. The former, i.e., the time necessary for particles to spread across the reactor from the feeding port, depends on the lateral sizes (L_x, L_y) of the reaction chamber according to[12]

$$t_{mix} \cong \frac{L_x L_y}{4D_r} \tag{15}$$

where D_r is a lateral fuel particle dispersion coefficient. Values of D_r for coarse fuel particles in the bottom bed of large-scale combustors have been estimated by Niklasson et al.[12] D_r is in the order of 0.1m^2/s[12–13] when dispersion of light fuel particles is promoted by "surface" migration due to bubble bursting. Smaller values of D_r are measured for particles fully immersed in the fluidized suspension.

A different approach must be followed to assess the lateral spreading of fuel particles that are fine enough to be readily entrained by the fluidizing gas on feeding. In this case the radial dispersion coefficient D_r is associated with turbulence inherent to the gas stream and expressed by the radial Peclet number[11]

$$Pe = \frac{UL}{D_r} \tag{16}$$

Values of Pe reported in the literature for dispersion of gases in the freeboard/riser of fluidized beds may be used to express the radial dispersion of very fine particles (Stokes number $\ll$ 1). If one takes $Pe \cong 300$,[11] it is

$$D_r \cong \frac{UL}{300} = 0.16 m^2/s \tag{17}$$

Computation of t_{mix} according to Eq. 15, assuming $L_x \cong L_y \cong 8$ m as the typical lateral size of a large-scale combustion chamber and $D_r \cong 0.1$ m^2/s, yields $t_{mix} \cong 10^2$ s, both for fine and coarse fuel particles.

The comparison between the fuel lateral mixing time (t_{mix}) for large-scale combustors/gasifiers and the devolatilization times (t_{D95}) is reported in Figure 13. The lateral mixing time t_{mix} is larger than t_{D95} for all the fuels investigated and for any particle size smaller than about 1 cm. This finding emphasizes the criticality of a proper matching of lateral

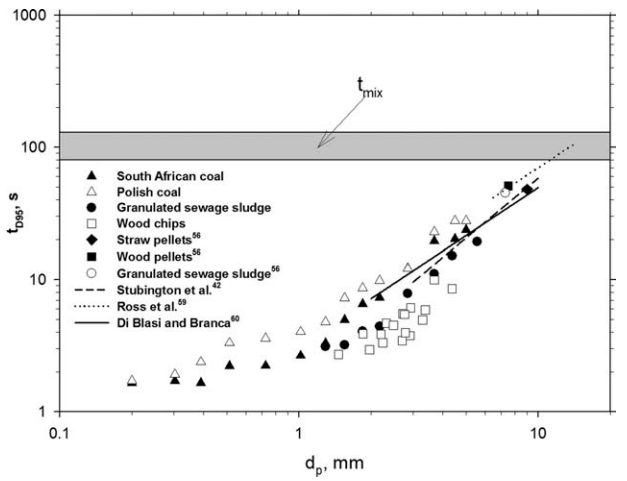

Figure 13. Devolatilization time as a function of the initial fuel particle size for all the fuels tested.- Lines refer to literature correlations.

The likely range of lateral fuel mixing times in large-scale fluidized-bed combustors is reported for comparison.

mixing times with devolatilization times as a prerequisite for achieving even release of volatile matter across the combustor. Fuel feedings should be kept relatively coarse (in the mm to cm range) to ensure that devolatilization times are of the same order as the lateral spreading times. On the other hand, convective transport of fuel particles, e.g., by purposely inducing net bulk flow of the fluidized suspension away from the fuel feeding point or by establishment of large-scale recirculation of the emulsion phase (''Gulf Stream''[69]) might be promoted to achieve even release of volatile matter across the combustor cross section.

The average molecular mass of emitted volatiles

The computed values of the mean molecular weight (M_{vol}) of the emitted volatile compounds are reported in Figures 9–12. It is recalled here that the procedure followed to compute M_{vol} from the raw pressure data yields a volume-averaged, rather than mass-averaged, molecular mass. This procedure emphasizes the contribution to M_{vol} of small molecular mass compounds (e.g., permanent gases, and in particular hydrogen, water, carbon mono- and dioxide and methane), as compared with large molecular mass compounds (e.g., tars). So, it is not surprising that the average molecular mass obtained for all the fuels tested are relatively small, falling in the range $10 < M_{vol} < 30$.

Data obtained with both raw and predried fuel batches are reported in Figures 9 and 12 for the South African coal and the wood chips, respectively. The influence of fuel pre-drying on the average molecular weight of the emitted volatiles is rather erratic and within the error limits.

No clear trend can be recognized in the M_{vol} vs. d_p plots for the bituminous coals (Figures 9 and 10), and the sludge pellets (Figure 11). Data referred to the wood chips (Figure 12) exhibit a moderately increasing trend of the average molecular mass of emitted volatiles vs. particle size. It might be inferred that the shift toward larger molecular mass could be related to enhanced effects of secondary pyrolysis as the fuel particle size increases.

Conclusions

A simple and reliable technique has been presented to measure the devolatilization rate of solid fuels of different nature at conditions relevant to fluidized-bed processing (combustion/gasification). The method is based on the analysis of overpressures induced by volatile matter release from a batch of fuel particles in a bench-scale fluidized-bed reactor, continuously vented to the atmosphere through a calibrated flow restriction. The operating conditions of the test procedure have been optimized, with the support of a mathematical model of the experiment, to determine the time-resolved devolatilization rate, the devolatilization time (t_{D95}), and the volume-based mean molecular weight (M_{vol}) of the emitted volatile compounds. An important and distinctive feature of the proposed method, as compared with alternative methods, is its inherently fine time-resolution that makes it possible to effectively follow also the fast devolatilization of fine ($0.1\ mm < d_p < 1\ mm$) fuel particles. The test protocol has been applied to different fuels (coals, granulated sewage sludge, wood chips) characterized by different initial particle sizes in the range 0.150–6 mm.

Experimental results confirm that devolatilization rate of mm-sized particles takes place in the thermally thick regime, and is controlled by heat transfer inside the fuel particle. Devolatilization of finer particles ($d_p < 1$ mm) is controlled to an increased extent by the intrinsic kinetics of pyrolytic processes.

The devolatilization time scales have been compared with the characteristic time scales of lateral spreading of fuel particles from the fuel feeding port in large-scale fluidized-bed combustors. The comparison underlines the criticality of lateral mixing of fuel particles, as a prerequisite for achieving even release of volatile matter across the reactor. A combination of relatively coarse fuel feedings (in the mm to cm size range) and measures for enhanced convective transport of fuel particles (e.g., net flow or Gulf stream of the fluidized suspension) may be effective to achieve this goal.

Acknowledgments

The support of Antonio Cammarota in the set up of the experimental apparatus and of Olga Narducci in the experimental campaign is gratefully acknowledged. The study has been carried out in the framework of the project MIUR-FISR.

Notation

A = constant of Eqs. 13 and 14, s/mm^n
d_p = particle size, mm
D_r = radial dispersion coefficient, m^2/s
K_p = proportionality constant of Eq. 1, m^3/s bar
L = characteristic length scale, m
L_x = lateral size of combustor chamber along x direction, m
L_y = lateral size of combustor chamber along y direction, m
m_s = fuel batch mass, g
m_v = mass of volatile matter, g
m_{v0} = initial mass of volatile matter, g
$\dot{m}_0$ = fluidizing gas mass flow rate, g/s
$\dot{m}_v$ = volatile matter mass flow rate, g/s
M_{gas} = molecular weight of the fluidizing gas, g/mol
M_{vol} = mean molecular weight of the volatile matter, g/mol
n = constant of Eq. 14, –
P = reactor pressure, bar
P_0 = steady-state reactor pressure, bar
P_{atm} = atmospheric pressure, bar
Q_{out} = exhaust flow rate, m^3/s
Q_{out0} = steady-state exhaust flow rate, m^3/s
R_g = gas constant, J/mol K
t = time, s
t_c = constant of Eq. 13, s
t_{D95} = characteristic devolatilization time,s
t_i = integration initial time, s
t_f = integration final time, s
T_R = reactor temperature, K
U = fluidization velocity, m/s
V_R = reactor volume, m^3

Greek letters

ρ_{gas} = mass concentration of fluidizing gas, kg/m^3
ρ_{gass} = steady-state mass concentration of fluidizing gas, kg/m^3
ρ_{IN} = density of fluidizing gas, kg/m^3
ρ_{vol} = mass concentration of volatile matter, kg/m^3
ρ_{vols} = steady-state mass concentration of volatile matter, kg/m^3
τ = time constant of Eq. 12, s
τ_f = time constant of differential Eq. 7, s

Dimensionless numbers

Pe = Peclet number

Literature Cited

1. Saxena SC. Devolatilization and combustion characteristics of coal particles. *Prog Energy Combust Sci*. 1990;16:55–94.
2. Fiorentino M, Marzocchella A, Salatino P. Segregation of fuel particles and volatile matter during devolatilition in a fluidized bed reactor. *Chem Eng Sci*. 1997;52:1893–1908.
3. Fiorentino M, Marzocchella A, Salatino P. Segregation of fuel particles and volatile matter during devolatilition in a fluidized bed reactor. *Chem Eng Sci*. 1997;52:1909–1922.
4. Nienow AW, Rowe PN. Fluidised Bed Mixing Segregation and Incineration in Solid Refuse Treatment. In: *Proc. 1st International Symposium on Mater Energy Refuse, Antwerp, Belgium*. 1976.
5. Yates JG, Macgillivray M, Cheesman, DJ. Coal devolatilization in fluidized bed combustors. *Chem Eng Sci*. 1980;35:2360–2361.
6. Atimtay A. *Combustion of volatile matter in fluidized beds*. In: Grace RJ, Matsen M, eds. *Fluidization*. New York: Plenum Press; 1980.
7. Pillai KK. The influence of coal type on devolatilization and combustion in fluidized beds. *J Inst Energy*. 1981;54:142–150.
8. Pillai KK. A schematic for coal devolatilization in fluidized bed combustors. *J Inst Energy*. 1982;55(424):132–133.
9. Bruni G, Solimene R, Marzocchella A, Salatino P, Yates JG, Lettieri P, Fiorentino M. Self-segregation of high-volatile fuel particles during devolatilization in a fluidized bed reactor. *Powder Technol*. 2002;128:11–21.
10. Solimene R, Marzocchella A, Salatino P. Hydrodynamic interaction between a coarser gas-emitting particle and a gas fluidized bed of finer solids. *Powder Technol*. 2003;133:79–90.
11. Luecke K, Hartge E-U, Werther J. A 3D model of combustion in large-scale circulating fluidized bed boilers. *Int J Chem Reactor Eng*. 2004;2:article A11:1–49.
12. Niklasson F, Thunman H, Johnsson F, Leckner B. Estimation of solids mixing in a fluidized-bed combustor. *Ind Eng Chem Res*. 2002;41:4663–4673.
13. Chirone R, Miccio F, Scala F. On the relevance of axial and transversal fuel segregation during the fluidized-bed combustion of a biomass. *Energy Fuels*. 2004;18(4):1108–1117.
14. LaNauze RD. Coal devolatilization in fluidized-bed combustors. *Fuel*. 1982;61:771–774.
15. Agarwal PK, Genetti WE, Lee YY. Model for devolatilization of coal particles in fluidized beds. *Fuel*. 1984;63:1157–1165.
16. Agarwal PK, Genetti WE, Lee YY. Devolatilization of large coal particles in fluidized beds. *Fuel*. 1984;63:1748–1752.
17. Agarwal PK, Genetti WE, Lee YY, Prasad SN. Model for drying during fluidized-bed combustion of wet low-rank coals. *Fuel*. 1984;63(7):1020–1027.
18. Agarwal PK. A single particle model for the evolution and combustion of coal volatiles. *Fuel*. 1986;65:803–810.
19. Devanathan N, Saxena SC. A model for the devolatilization of large coal particle. *Chem Eng Sci*. 1986;41:2442–2446.
20. Chirone R. [PhD Thesis]. Primary fragmentation of coal during fluidized bed combustion. Università degli studi di Napoli Federico II, Napoli, Italy, 1986.
21. Agarwal PK, Wildegger-Gaissmaier AE. Combustion of coal volatiles in gas fluidized beds. *Chem Eng Res Des*. 1987;65(5):431–441.
22. Chirone R, Massimilla L. *Primary fragmentation of a coal in fluidized bed combustion*. In: *22nd International Symposium on Combustion*. Pittsburgh, PA: The Combustion Institute; 1988.
23. Misra MK, Essenhigh RH. Release of volatiles from pyrolyzing coal particles: relative roles of kinetics, heat transfer, and diffusion. *Energy Fuels*. 1988;2:371–385.
24. Kilic YA, Kahveci N, Dincer I, Bardakci T. An experimental and theoretical investigation of transient heat transfer between a spherical coal particle and air medium during devolatilization. *Int Com Heat Mass Transfer*. 1993;20(5):711–720.
25. Adesanya BA, Pham HN. Mathematical modeling of devolatilization of large coal particles in a convective environment. *Fuel*. 1995;74(6):896–902.
26. Sasongko D, Stunington JF, Significant factors affecting devolatilization of fragmenting, non-swelling coals in fluidized bed combustion. *Chem Eng Sci*. 1996;51:3909–3918.
27. Stubington JF, Sasongko D. On the heating rate and volatile yield for coal particles injected into fluidized bed combustors. *Fuel*. 1998;77(9/10):1021–1025.
28. Di Felice R, Coppola G, Rapagnà S, Jand N. Modeling of biomass devolatilization in a fluidized bed reactor. *Can J Chem Eng*. 1999;77:325–332.
29. de Diego LF, Garcia-Labiano F, Abad A, Gayan P, Adanez J. Modeling of the devolatilization of nonspherical wet pine wood particles in fluidized beds. *Ind Eng Chem Res*. 2002;41:3642–3650.
30. de Diego LF, Garcia-Labiano F, Abad A, Gayan P, Adanez J. Effect of moisture content on devolatilization times of pine wood particles in a fluidized bed. *Energy Fuels*. 2003;17(2):285–290.
31. Thunman H, Davidsson K, Leckner B. Separation of drying and devolatilization during conversion of solid fuels. *Combust Flame*. 2004;137(1/2):242–250.
32. Chern J-S, Hayhurst Allan N. Does a large coal particle in a hot fluidised bed lose its volatile content according to the shrinking core model? *Combust Flame*. 2004;139(3):208–221.
33. Saastamoinen JJ. Simplified model for calculation of devolatilization in fluidized beds. *Fuel*. 2006;85(17–18):2388–2395.
34. Chern J-S, Hayhurst AN. A model for the devolatilization of a coal particle sufficiently large to be controlled by heat transfer. *Combust Flame*. 2006;146(3):553–571.
35. Sreekanth M, Sudhakar DR, Prasad BVSSS, Kolar AK, Leckner B. Modelling and experimental investigation of devolatilizing wood in a fluidized bed combustor. *Fuel*. 2008;87(12):2698–2712.
36. Sreekanth M, Kolar AK, Leckner B. Transient thermal behaviour of a cylindrical wood particle during devolatilization in a bubbling fluidized bed. *Fuel Proc Tech*. 2008;89(9):838–850.
37. Anthony DB, Howard JB, Hottel HC, Meissner HP. *Rapid devolatilization of pulverized coal*. In: *Fifteenth International Symposium on Combustion*. Pittsburgh, Pa: The Combustion Institute; 1975.
38. Anthony DB, Howard JB. Coal devolatilization and hydrogasification. *AIChE J*. 1976;22:625.
39. Howard JB. *Fundamentals of coal pyrolysis and hydropyrolysis*. In: Elliott MA, ed. *Chemistry of Coal Utilization*. 2nd vol. New York: Wiley & Sons, Inc; 1981:665–784.
40. Peeler JPK, Poynton HJ, Lane GL, Ahmed S. Fluidized-bed combustion: devolatilization of large coal particles. In: Proceedings of the 11th International Conference on Fluidized Bed Combustion, Montreal, Canada; 1991:1.
41. Stubington JF, Huang G, Scaroni AW. Devolatilization times of mm-size coal particles. *Fuel*. 1991;70:1105–1108.
42. Stubington JF, Ng KWK, Moss B, Peeler PK. Comparison of experimental methods for determining coal particle devolatilization times under fluidized bed combustor conditions. *Fuel*. 1997;76:233–240.
43. Eatough CN, Smoot LD. Devolatilization of large coal particles at high pressure. *Fuel*. 1996;75(13):1601–1605.
44. Pillai KK. Devolatilization and combustion of large coal particles in a fluidized bed. *J Inst Energy*. 1985;58:3–7.
45. Prins W, Siemons R, Van Swaaij WPM. Devolatilization and ignition of coal particles in a two-dimensional fluidized bed. *Combust Flame*. 1989;75:57–79.
46. Zhang JQ, Becker HA, Code RK. Devolatilization and combustion of large coal particles in a fluidized bed. *Can J Chem Eng*. 1990;68:1010–1017.
47. Urkan MK, Arikol M. Burning times of volatiles from Turkish coals during fluidized bed combustion. *Fuel*. 1994;73:768–772.
48. Winaya INS, Shimizu T. Reduction of the volatile matter evolution rate from a plastic pellet during bubbling fluidized bed pyrolysis by using porous bed material. *Chem Eng Tech*. 2007;30(8):1003–1009.
49. Jung K, Stanmore BR. Fluidized bed combustion of wet brown coal. *Fuel*. 1980;59:74–80.
50. Morris JP, Keairns DL. Coal devolatilization studies in support of the Westinghouse fluidized-bed coal gasification process. *Fuel*. 1979;58:465–471.
51. Stubington JF, Sumaryono. Release of volatiles from large coal particles in a hot fluidized bed. *Fuel*. 1984;63:1013–1019.
52. Salam TF, Shen XL, Gibbs BM. A technique for determining devolatilization rates of large coal particles in a fluidized bed combustor. *Fuel*. 1988;67:414–419.
53. de Diego LF, Gracia-Labiano AA, Gayan P, Adanez J. Coupled drying and devolatilisation of non-spherical wet pine wood particles in fluidised beds. *J Anal Appl Pyrolysis*. 2002;65(2):173.184.
54. Jand N, Foscolo PU. Decomposition of wood particles in fluidized beds. *Ind Eng Chem Res*. 2005;44(14):5079–5089.

55. Scott SA, Davidson JF, Dennis JS, Hayhurst AN. The devolatilization of particles of a complex fuel (dried sewage sludge) in a fluidized bed. *Chem Eng Sci*. 2007;62(1–2):584–598.
56. Chirone R, Salatino P, Scala F, Solimene R, Urciuolo M. Fluidized bed combustion of pelletized biomass and waste-derived fuels. *Combust Flame*. 2008;155(1/2):21–36.
57. Gomez-Barea A, Nilsson S, Vidal Barrero F, Campoy M. Devolatilization of wood and wastes in fluidized bed. *Fuel Process Technol*. 2010;91:1624–1633.
58. Heidenreich CA, Zhang DK. Measuring the temperature response of large wet coal particles during heating. *Fuel*. 1999;78(8):991–994.
59. Ross DP, Heidenreich CA, Zhang DK. Devolatilisation times of coal particles in a fluidised-bed. *Fuel*. 2000;79:873–883.
60. Di Blasi C, Branca C. Temperatures of wood particles in a hot sand bed fluidized by nitrogen. *Energy Fuels*. 2003;17(1):247–254.
61. Jand N. [PhD Thesis]. Biomass gasification in fluidized bed for the production of hydrogen and syngas. Università degli studi di Napoli Federico II, Napoli, Italy, 1998.
62. Broadhurst TE, Becker HA. Onset of fluidization and slugging in beds of uniform particles. *AIChE J*. 1975;21:238–247.
63. Wen CY, Yu YH. A generalized method for predicting the minimum fluidization velocity. *AIChE J*. 1966;12:610–612.
64. Chirone R, Massimilla L. The application of Weibull theory to primary fragmentation of a coal during devolatilization. *Power Technol*. 1989;57:197–212.
65. Salatino P. Work-package 2 Fuel characterization of biomass and waste materials. In: *Synergy Effects of Co-processing of Biomass with Coal and Non-Toxic Wastes for Heat and Power Generation*. EU Contract no. SES6-CT-2004–503806, final technical report; 2006.
66. Scala F, Chirone R, Salatino P. Combustion and attrition of biomass chars in a fluidized bed. *Energy Fuels*. 2006;20:91–102.
67. Niksa S, Russel WB, Saville DA. Time-resolved weight loss kinetics for the rapid devolatilization of a bituminous coal. In: *Proceedings of Symposium International on Combustion, Haifa, Israel*. 1982;19:1151–1157.
68. Solomon PR, Serio MA, Suuberg EM. Coal pyrolysis: experiments, kinetic rates and mechanisms. *Prog Energy Comb Sci*. 1992;18:133–220.
69. Merry JMD, Davidson JF. "Gulf Stream" circulation in shallow fluidised beds. *Trans Inst Chem Eng*. 1973;51:361–368.

Manuscript received Aug. 10, 2010, and revision received Feb. 4, 2011.